International Forum on Aeroelasticity and Structural Dynamics
IFASD 2019
9-13 June 2019, Savannah, Georgia, USA

A STATE-SPACE MODEL FOR LOADS ANALYSIS BASED ON TANGENTIAL INTERPOLATION

David Quero[1], Christoph Kaiser[1], Pierre Vuillemin[2], Charles Poussot-Vassal[2]

[1]Institute of Aeroelasticity, DLR (German Aerospace Center)
Bunsenstraße 10, 37073 Göttingen, Germany
David.QueroMartin@dlr.de

[2]DTIS (Information Processing and Systems), ONERA (French Aerospace Lab)
Université de Toulouse, 31055 Toulouse, France

Keywords: Aeroservoelasticity, reduced order model, Loewner framework, tangential interpolation, gust load alleviation, H_∞ controller synthesis

Abstract: In this work an approach for the generation of a generalized state-space aeroservoelastic model based tangential interpolation, also known as Loewner rational interpolation, is presented. The resulting differential algebraic system (DAE) system is reduced to a set of ordinary differential equations (ODE) by residualization of the non-proper part of the transfer function matrix. The generalized state-space is of minimal order and allows for the application of the force summation method (FSM) for the aircraft loads recovery, which shows a superior convergence when compared to the mode displacement method (MDM) for an increasing number of generalized coordinates for the cut loads recovery. Compared to the classical rational function approximation (RFA) approach, the presented method provides a minimal order realization with exact interpolation of the unsteady aerodynamic forces in tangential directions, avoiding any selection of poles (lag states). After a demonstration of the tangential interpolation techniques on the transcendental Theodorsen and Sears functions, the new approach is applied to the generation of an aeroservoelastic model for loads evaluation of the NASA Common Research model under atmospheric disturbances, showing an excellent agreement with the reference model in the frequency domain. Applications include the aerodynamic transfer function matrices generated by either potential flow or linearized computational fluid dynamics (CFD) solvers. The resulting aeroservoelastic model of minimal order is used for the design of an H_∞-optimal controller for gust loads alleviation (GLA).

1 INTRODUCTION

One of the major tasks for aircraft certification is the consideration of dynamic load cases, in particular those caused by gust and continuous turbulence encounters, considered by the regulatory agencies [1, 2]. In order to reduce the internal loads caused by these atmospheric disturbances without compromising the structural weight different load alleviation schemes are applied. To that aim, an accurate model suited for the design of advance control laws covering the complete flight envelope is of most relevance. Thus the need arises for a precise but at the same time efficient model description in order to develop suitable control laws for an efficient load reduction when encountering atmospheric disturbances. Moreover, modern transport aircraft are becoming more flexible and as a result the eigenfrequency values corresponding to the

first flexible modes decrease and tend to interact with the rigid-body behaviour of the structure, requiring thus a model description containing both the rigid and flexible effects for an effective load alleviation.

Modern approaches of control theory require a description of the model in the time domain of minimum size. However, the aerodynamic models describing the flow over the aircraft are provided within the frequency domain in tabular form as they cannot usually be obtained in an explicit form and if they do, they contain transcendental functions which cannot be transformed in the time domain by a direct application of an inverse Laplace transform. Thus there is a need of converting the frequency domain description into time domain models.

The method of Roger [3] and Abel [4] represents the three-dimensional unsteady subsonic aerodynamic flow by means of a least-squares technique with a series of poles which represent the aerodynamic lags due to the presence of the wake. All elements of the transfer function matrix share the same poles, which in turn have to be chosen in advance. Note that the least squares fit is ill-conditioned when increasing the number of real poles and prone to numerical instabilities [5, 6]. For the representation of a gust excitation additional issues related to the time delay behaviour are encountered. In order to take into account the poles as parameters to the least-squares fit they can be further considered in an optimization problem [7, 8], ensuring a minimum error of the least-squares for a fixed number of poles. Karpel presented the minimum-state method [9], where an iterative least-squares process is applied to the aeroelastic system, reducing the total number of augmented states. This iterative process leads to a significantly increase of the computational effort which may be of up to three orders of magnitude [10].

In an effort to reduce the size of the aeroservoelastic systems formulated in the time domain, modern techniques of the control theory have been commonly applied to aeroelastic systems where the loads recovery is done by means of the mode displacement method (MDM) [11–14], even though the force summation method (FSM) method has a superior convergence of the cut loads values with respect to the number of structural modes considered. In this work the FSM method is considered for the recovery of the cut loads acting over the airframe, both in the time and in the frequency domains.

In general all the rational function approximation (RFA) methods introduce an error in the description of the aerodynamic loads due to the least squares fit. In order to avoid this error, different techniques based on rational *interpolation* may be used. More recently, the eigensystem realization algorithm (ERA) algorithm [15] has been widely used for system identification and model reduction [16, 17] in the time domain, which presents two main limitations. Firstly, its application is limited to systems with a proper transfer function matrix and thus only the MDM method can be considered for the loads recovery. Secondly, if the system under consideration has a large number of inputs and outputs then a big computational effort is required to compute the singular value decomposition (SVD) of the dense Hankel matrix [18].

For the consideration of linear time invariant (LTI) multi-input multi-output (MIMO) systems with non-proper transfer function matrix a more general setting, namely that of the linear descriptor systems, is needed [19]. The approach presented in this work is based on the Loewner framework for descriptor systems, which represents an extension of the rational interpolation at infinite frequency to a set of frequencies available at particular values [20].

In this work an approach to generate an aeroservoelastic state-space model suited for loads computation and control design which overcomes the above limitations and listed in Table 1

Formulation	Method	Limitations
Roger (1977) [3]	Rational functional approximation (RFA) with fixed real poles	-Use of real poles, lack of complex poles to represent oscillatory fluid modes typical in the transonic regime. -Increasing the number of poles may result in an ill-conditioned problem. -Not appropriate for input delays (gust)
Karpel (1982) [9]	Rational functional approximation (RFA) and nonlinear optimization	-Use of real poles, lack of complex poles to represent oscillatory fluid modes typical in the transonic regime. -Very high computational time. -Not appropriate for input delays (gust)
Silva (2004) [16]	Eigensystem realization algorithm (ERA)	-Rigid-body modes are not considered. -It requires a proper aerodynamic transfer function matrix. -Computation of the Hankel matrix.
Brunton (2014) [21]	Eigensystem realization algorithm (ERA)	-Non-proper part of the aerodynamic transfer function matrix must be explicitly known. -Computation of the Hankel matrix.

Table 1: Summary of methods applied for the formulation of aerodynamic and aeroservoelastic models in the time domain and current limitations.

is presented. The proposed approach shall overcome all the current limitations, avoiding any selection of poles. Also, no iterative procedure is required for the precise formulation of the aeroservoelastic model in the time domain.

Regarding the design of proper controllers for load reduction, several methods have been applied for the design of GLA techniques [22, 23]. In the present work a feedback controller strategy based on measurements over the aircraft structure has been considered. The aeroservoelastic model presented in this work allows for the systematic consideration of the flexible effects into the controller design, which have been shown to play a role due to the interaction with the rigid-body behaviour of the aircraft [24, 25]. Aouf et al. [26] compared the effectivity of different controllers designed with H_2, weighted-H_2 and H_∞ techniques, showing the superiority of both the weighted-H_2 and H_∞ controllers when compared to a regular H_2 design. Typically the available sensor measurements for the controller action are either structural displacements, velocities or accelerations. The aim of this work concerns the generation of a proper aeroservoelastic model and thus it is assumed that the wing root bending moment can be directly measured, leading to the design of an optimal H_∞ controller which makes use of the outer ailerons for the load reduction strategy. Additional sensors and actuators can be readily added to the developed model [27].

The paper is organized as follows. In Section 2 the Loewner realization in connection with the theory of descriptor linear systems is presented and an application to the bidimensional unsteady incompressible flow over an airfoil containing transcendental functions is shown. A generalization to three-dimensional aeroservoelastic systems is then presented in Section 3. In Section 4 applications to the NASA common research model (CRM) / flutter reduced order assessment (FERMAT) model with aerodynamic models considering the doublet lattice (DLM)

potential method and high-fidelity CFD methods are presented. Additionally, an H_∞-optimal controller for a GLA strategy is developed. Finally conclusions and future work are pointed out in Section 5.

2 GENERALIZED REALIZATION PROBLEM

2.1 Tangential interpolation

A descriptor linear system $\boldsymbol{\Sigma}$ is described in the time domain by a set of differential and algebraic equations (DAE), also denoted as generalized state-space system:

$$\begin{aligned} \boldsymbol{\Sigma}: \ \mathbf{E}\dot{\mathbf{x}}(t) &= \mathbf{A}\mathbf{x}(t) + \mathbf{B}\mathbf{u}(t) \\ \mathbf{y}(t) &= \mathbf{C}\mathbf{x}(t) + \mathbf{D}\mathbf{u}(t), \end{aligned} \tag{1}$$

where $\mathbf{x}(t) \in \mathbb{R}^n$ is the state vector, $\mathbf{u}(t) \in \mathbb{R}^{n_u}$ the input vector, $\mathbf{E}, \mathbf{A} \in \mathbb{R}^{n \times n}$, $\mathbf{B} \in \mathbb{R}^{n \times n_u}$, $\mathbf{C} \in \mathbb{R}^{n_y \times n}$ and $\mathbf{D} \in \mathbb{R}^{n_y \times n_u}$ are constant with $\mathbf{E}$ possibly singular. In this work regular systems are considered, that is, $\det(s\mathbf{E} - \mathbf{A}) \neq 0$ except for a finite number of eigenvalues (which may have an infinite value), denoted by the set $\sigma(\mathbf{E}, \mathbf{A})$. The resolvent set $\rho(\mathbf{E}, \mathbf{A})$ is given by $\rho(\mathbf{E}, \mathbf{A}) = \mathbb{C} \setminus \sigma(\mathbf{E}, \mathbf{A})$.

The transfer function matrix $\mathbf{H}(s)$ of the system $\boldsymbol{\Sigma}$ is:

$$\mathbf{H}(s) = \mathbf{C}(s\mathbf{E} - \mathbf{A})^{-1}\mathbf{B} + \mathbf{D},$$

and is said to be proper if $\lim_{s\to\infty} \mathbf{H}(s)$ is bounded ($< \infty$ for each of the its components) and strictly proper if $\lim_{s\to\infty} \mathbf{H}(s) = \mathbf{0}$. If the DAE system is split into the fast $\mathbf{H}_\infty(s)$ (including only the poles with infinite value) and slow subsystems $\mathbf{H}_p(s)$ (including only the finite poles) and restricted system equivalence relations are applied so that $\mathbf{H}(s) = \mathbf{H}_p(s) + \mathbf{H}_\infty(s)$, the non-proper part of the transfer function matrix $\mathbf{H}_\infty(s)$ can be written as a Neumann series expansion [28]:

$$\mathbf{H}_\infty(s) = \mathbf{C}(s\mathbf{N} - \mathbf{I})^{-1}\mathbf{B} + \mathbf{D} = \mathbf{D} - \mathbf{C}\mathbf{B} - \sum_{j=1}^{v-1} s^j \mathbf{C}\mathbf{N}^j\mathbf{B},$$

where $\mathbf{N}$ is a nilpotent matrix with nilpotence index v and coincides with the DAE index. This provides a direct relation between the so called DAE index v and the non-proper part of the transfer function matrix $\mathbf{H}_\infty(s)$, with the DAE index ν one order less than that of the highest polynomial term.

The set $(\mathbf{E}, \mathbf{A}, \mathbf{B}, \mathbf{C}, \mathbf{D})$ is called a realization of $\mathbf{H}(s)$. The realization is not unique and the one of the smallest possible order n is called minimal. The minimal realization used here is based on the rational interpolation for tangential data [19,29]. Tangential interpolation is a form of rational interpolation where the data is interpolated along particular directions. In particular, the data consist of the right interpolation data:

$$\left\{\lambda_i, \mathbf{r}_i, \mathbf{w}_i \mid \lambda_i \in \mathbb{C}, \mathbf{r}_i \in \mathbb{C}^{n_y \times 1}, \mathbf{w}_i \in \mathbb{C}^{n_u \times 1}\right\},$$

for $i = 1, ..., n_r$:

$$\begin{aligned}
\mathbf{\Lambda} &= \text{diag}\left[\lambda_1, ..., \lambda_{n_r}\right] \in \mathbb{C}^{n_r \times n_r} \\
\mathbf{R} &= \left[\mathbf{r}_1, ..., \mathbf{r}_{n_r}\right] \in \mathbb{C}^{n_u \times n_r} \\
\mathbf{W} &= \left[\mathbf{w}_1, ..., \mathbf{w}_{n_r}\right] \in \mathbb{C}^{n_y \times n_r},
\end{aligned}$$

and the left interpolation data:

$$\left\{\mu_j, \mathbf{l}_j, \mathbf{v}_j \mid \mu_j \in \mathbb{C}, \mathbf{l}_j \in \mathbb{C}^{1\times n_u}, \mathbf{v}_j \in \mathbb{C}^{1\times n_y}\right\},$$

for $j = 1, ..., n_l$:

$$\begin{aligned}
\mathbf{M} &= \text{diag}\left[\mu_1, ..., \mu_{n_l}\right] \in \mathbb{C}^{n_l \times n_l} \\
\mathbf{L} &= \left[\mathbf{l}_1^T, ..., \mathbf{l}_{n_l}^T\right]^T \in \mathbb{C}^{n_l \times n_y} \\
\mathbf{V} &= \left[\mathbf{v}_1^T, ..., \mathbf{v}_{n_l}^T\right]^T \in \mathbb{C}^{n_l \times n_u}.
\end{aligned}$$

The transfer function matrix is evaluated at the values λ_i, μ_j and $\mathbf{r}_i, \mathbf{l}_j$ are referred to as right and left tangential directions, while $\mathbf{w}_i, \mathbf{v}_j$ are the right and left tangential data. The rational interpolation problem for tangential data aims at finding a realization $(\mathbf{E}, \mathbf{A}, \mathbf{B}, \mathbf{C}, \mathbf{D})$ such that the associated transfer function $\mathbf{H}$ satisfies the right and left constraints,

$$\begin{aligned}
&\mathbf{H}\left(\lambda_i\right)\mathbf{r}_i = \mathbf{w}_i, \quad i = 1, ..., n_r \\
&\mathbf{l}_j\mathbf{H}\left(\mu_j\right) = \mathbf{v}_j, \quad j = 1, ..., n_l
\end{aligned} \tag{2}$$

which is achieved by means of the Loewner and shifted Loewner matrices. Next the structure of these two matrices is described.

The set Z of points in the complex plane $Z = \left\{z_1, ...z_{n_r+n_l}\right\}$ and the corresponding values of the transfer function matrix is partitioned into the left and right data:

$$Z = \left\{\lambda_1, ..., \lambda_{n_r}\right\} \cup \left\{\mu_1, ..., \mu_{n_l}\right\}, \tag{3}$$

where the total number of sample points is $n_r + n_l$. The Loewner matrix is built as:

$$\mathbb{L} = \begin{bmatrix} \frac{\mathbf{v}_1\mathbf{r}_1 - \mathbf{l}_1\mathbf{w}_1}{\mu_1 - \lambda_1} & \cdots & \frac{\mathbf{v}_1\mathbf{r}_{n_r} - \mathbf{l}_1\mathbf{w}_{n_r}}{\mu_1 - \lambda_{n_r}} \\ \vdots & \ddots & \vdots \\ \frac{\mathbf{v}_{n_l}\mathbf{r}_1 - \mathbf{l}_{n_l}\mathbf{w}_1}{\mu_{n_l} - \lambda_1} & \cdots & \frac{\mathbf{v}_{n_l}\mathbf{r}_{n_r} - \mathbf{l}_p\mathbf{w}_{n_r}}{\mu_{n_l} - \lambda_{n_r}} \end{bmatrix},$$

The Loewner matrix can be also expressed in terms of the tangential controllability and observability matrices [29]. If the directions $\mathbf{r}_i, \mathbf{l}_j$ are selected generically (random in practice) the rank of the Loewner matrix $\mathbb{L}$ is equal to the rank of the underlying matrix $\mathbf{E}$. The shifted Loewner matrix is the Loewner matrix corresponding to $s\mathbf{H}\left(s\right)$ and is built as:

$$\mathbb{L}_\sigma = \begin{bmatrix} \frac{\mu_1\mathbf{v}_1\mathbf{r}_1 - \lambda_1\mathbf{l}_1\mathbf{w}_1}{\mu_1 - \lambda_1} & \cdots & \frac{\mu_1\mathbf{v}_1\mathbf{r}_{n_r} - \lambda_{n_r}\mathbf{l}_1\mathbf{w}_{n_r}}{\mu_1 - \lambda_{n_r}} \\ \vdots & \ddots & \vdots \\ \frac{\mu_{n_l}\mathbf{v}_{n_l}\mathbf{r}_1 - \lambda_1\mathbf{l}_{n_l}\mathbf{w}_1}{\mu_{n_l} - \lambda_1} & \cdots & \frac{\mu_{n_l}\mathbf{v}_{n_l}\mathbf{r}_{n_r} - \lambda_{n_r}\mathbf{l}_{n_l}\mathbf{w}_{n_r}}{\mu_{n_l} - \lambda_{n_r}} \end{bmatrix},$$

Assuming that $n_r = n_l$ and that $\det\left(\mathbb{L}_\sigma - s\mathbb{L}\right) \neq 0$ a minimal realization for the linear descriptor system is given by [19, 30]:

$$\mathbf{E} = -\mathbb{L},\ \mathbf{A} = -\mathbb{L}_\sigma,\ \mathbf{B} = \mathbf{V},\ \mathbf{C} = \mathbf{W},\ \mathbf{D} = \mathbf{0}, \tag{4}$$

and the associated transfer function $\mathbf{H}(s) = \mathbf{W}\left(\mathbb{L}_\sigma - s\mathbb{L}\right)^{-1}\mathbf{V}$ satisfies the right and left interpolation conditions of Eq. 2. An additional SVD factorization of the Loewner matrix $\mathbb{L}$ allows for the further size reduction of the system, generating a reduced order model (ROM) of the descriptor system:

$$\mathbb{L} = \begin{bmatrix} \mathbf{Y}_1 & \mathbf{Y}_2 \end{bmatrix} \begin{bmatrix} \mathbf{S}_1 & \mathbf{0} \\ \mathbf{0} & \mathbf{S}_2 \end{bmatrix} \begin{bmatrix} \mathbf{X}_1^* \\ \mathbf{X}_2^* \end{bmatrix}, \tag{5}$$

where $*$ denotes the conjugate transpose, $\mathbf{S}_1 \in \mathbb{R}^{r\times r}$, $\mathbf{S}_2 \in \mathbb{R}^{(n-r)\times(n-r)}$ and $\mathbf{X}_1, \mathbf{X}_2, \mathbf{Y}_1, \mathbf{Y}_2$ are of appropriate dimensions. The reduced system of size r defined by $(\mathbf{E}_r, \mathbf{A}_r, \mathbf{B}_r, \mathbf{C}_r, \mathbf{D}_r)$ is obtained by a Petrov-Galerkin projection and represents the best approximation to the full Loewner matrix in the Frobenius or 2-norm:

$$\mathbf{E}_r = -\mathbf{Y}_1^*\mathbb{L}\mathbf{X}_1,\ \mathbf{A}_r = -\mathbf{X}_1^*\mathbb{L}_\sigma\mathbf{X}_1,\ \mathbf{B}_r = \mathbf{Y}_1^*\mathbf{V},\ \mathbf{C}_r = \mathbf{W}\mathbf{X}_1,\ \mathbf{D}_r = \mathbf{0}. \tag{6}$$

Once the set $(\mathbf{E}_r, \mathbf{A}_r, \mathbf{B}_r, \mathbf{C}_r, \mathbf{D}_r)$ has been determined, this system may contain unstable poles. Assuming that the aeroelastic system under consideration is stable, the system is then approximated by a stable one. This is done by means of an approximation in the Hardy space H_∞ [30, 31].

2.2 Application to transcendental aerodynamic transfer functions

The main task for the application of the FSM method for the cut loads recovery in an aeroservoelastic framework remains to properly describe the distributed unsteady aerodynamic forces in the time domain. In order to show the convenience of the tangential interpolation method described in Section 2.1 an application for the incompressible unsteady flow over a bidimensional profile with heave and pitch degrees of freedom is presented. Based on this application, a connection between the theory of DAE or descriptor systems and the unsteady aerodynamic flow is shown. In Section 2.2.2 including atmospheric disturbances is considered.

The classical unsteady model of Theodorsen [32] provides the lift and pitch moment coefficient (excluding the added-mass terms) to arbitrary input motions of the profile under the assumptions of inviscid flow, incompressibility and planar wake. As described by Brunton [33], several authors have constructed state-space models corresponding to the Theodorsen formulation. Note that excluding the models obtained by Peters [34], which requires up to eight states for an appropriate system representation, these state-space formulations do not include the added-mass terms. In this section a time domain model including also the added-mass terms is presented.

The total local lift c_l (positive upwards) and local pitch moment at the quarter chord c_m (positive nose up) can be described as function of the heave u_z (positive down) and pitch u_θ (positive nose up) motion in the frequency domain by means of an aerodynamic transfer function matrix:

$$\begin{bmatrix} c_l(\omega) \\ c_m(\omega) \end{bmatrix} = \mathbf{H}_t(\omega) \begin{bmatrix} u_z(\omega) \\ u_\theta(\omega) \end{bmatrix},$$

where the system output is $\mathbf{y} = \begin{bmatrix} c_l & c_m \end{bmatrix}^T$, the system input $\mathbf{u} = \begin{bmatrix} u_z & u_\theta \end{bmatrix}^T$ and the transfer function matrix is [35]:

$$\mathbf{H}_t(\omega) = \begin{bmatrix} -\omega^2 \frac{\pi L_{ref}}{U_\infty^2} + i\omega \frac{2\pi}{U_\infty} C(k) & \omega^2 \frac{\pi a L_{ref}^2}{U_\infty^2} + i\omega \frac{\pi L_{ref}}{U_\infty} (1 + (1-2a) C(k)) + 2\pi C(k) \\ \omega^2 \frac{\pi L_{ref}}{4U_\infty^2} & \omega^2 \left(\frac{1}{8} - \frac{a}{2}\right) \frac{\pi L_{ref}^2}{2U_\infty^2} - i\omega \frac{\pi L_{ref}}{2U_\infty} \end{bmatrix}, \tag{7}$$

with k the reduced frequency $k = \omega L_{ref}/U_\infty$, where L_{ref} is a reference length (the half-chord) and U_∞ the true airspeed. The parameter a represents the pitch axis location with respect to the half-chord and ranges between -1 for the leading edge and 1 for the trailing edge. The Theodorsen function $C(k)$ is given by

$$C(k) = \frac{H_1^{(2)}(k)}{H_1^{(2)}(k) + iH_0^{(2)}(k)},$$

with H_0 and H_1 the Hankel functions of first and second kind [32]. Interestingly, the pitch moment at the quarter chord position is independent of the Theodorsen function.

It is clear from Eq. 7 that the aerodynamic system is not proper, as the values $\lim_{s\to\infty} \mathbf{H}(s)$ are not bounded. According to the description of Section 2.1 and to Eq. 7, the corresponding time domain description must be in the form of a descriptor system of index $\upsilon = 3$. In Quero et al. [30] a strategy for the application of the Loewner realization to this aerodynamic system together with a reduction of the DAE index in order to obtain a regular ODE system including the time derivatives of the input has been presented.

In the case of bidimensional incompressible flow the DAE of index 3 can been reduced to a regular ODE provided the time derivatives of first and second order of the input signal are included. For compressible flow and due to the behaviour of the aerodynamic solvers at high frequencies this cannot be done in a straightforward manner and thus the dependence of the unsteady aerodynamic forces on the second time derivative resulting from the classical RFA fit [3] for compressible flow may be seen as a low frequency residualization of its high frequency behaviour [27].

Next the proposed Loewner realization is applied to two well-known transcendental aerodynamic transfer functions corresponding to the unsteady motion-induced and gust-induced aerodynamic incompressible flow, namely the Theodorsen function in Section 2.2.1 and the Sears function in Section 2.2.2.

2.2.1 Theodorsen function

In the case of bidimensional unsteady incompressible flow a general realization can be obtained which is then valid for all values of the parameters involved in Eq. 7, namely U_∞, L_{ref} and a. For a realization of the Theodorsen function the following strictly proper aerodynamic transfer function is defined:

$$H_c(k) = C(k) - \frac{1}{2},$$

where $C(k)$ represents the Theodorsen function which depends on the reduced frequency k. Next the Loewner and shifted Loewner matrices are built and a realization is carried out:

$$\mathbf{A}_c = \mathbf{E}_{cr}^{-1}\mathbf{A}_{cr},\ \mathbf{B}_c = \mathbf{E}_{cr}^{-1}\mathbf{B}_{cr},\ \mathbf{C}_c = \mathbf{E}_{cr}^{-1}\mathbf{C}_{cr},\ \mathbf{D}_c = \mathbf{E}_{cr}^{-1}\mathbf{D}_{cr} = \mathbf{0},$$

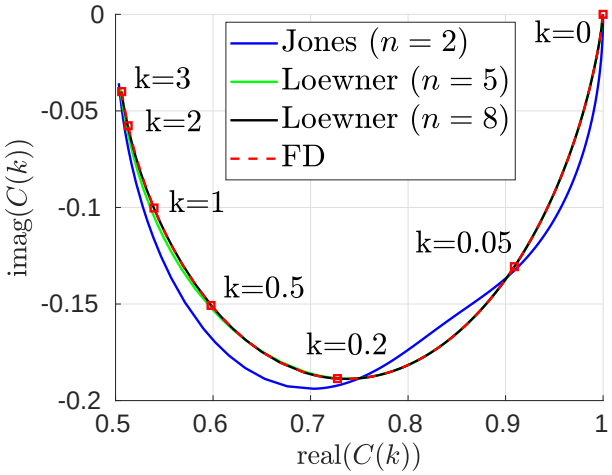

Figure 1: Theodorsen function in the complex plane and corresponding Jones and Loewner approximations.

where the system $(\mathbf{E}_{cr}, \mathbf{A}_{cr}, \mathbf{B}_{cr}, \mathbf{C}_{cr}, \mathbf{D}_{cr})$ is obtained after applying Eqs. 4 and 6 for a reduction on the number of states and a projection on the Hardy space H_∞ for the suppression of possible unstable poles on the aerodynamic transfer function H_c. The resulting generalized state-space system is:

$$\dot{\mathbf{x}}_c = \mathbf{A}_c \mathbf{x}_c + \mathbf{B}_c \frac{2\pi}{U_\infty} \begin{bmatrix} 0 & U_\infty & 1 & L_{ref}\left(\frac{1}{2} - a\right) & 0 & 0 \end{bmatrix} \begin{bmatrix} \mathbf{u} \\ \dot{\mathbf{u}} \\ \ddot{\mathbf{u}} \end{bmatrix}$$

$$\begin{bmatrix} c_l \\ c_m \end{bmatrix} = \begin{bmatrix} \mathbf{C}_c \\ \mathbf{0} \end{bmatrix} \mathbf{x}_c + \left(\begin{bmatrix} 0 & \pi & \frac{\pi}{U_\infty} & \frac{\pi L_{ref}}{U_\infty}\left(\frac{3}{2} - a\right) & \frac{\pi L_{ref}}{U_\infty^2} & -\frac{\pi a L_{ref}^2}{U_\infty^2} \\ 0 & 0 & 0 & -\frac{\pi L_{ref}}{2U_\infty} & -\frac{\pi L_{ref}}{4U_\infty^2} & -\left(\frac{1}{8} - \frac{a}{2}\right)\frac{\pi L_{ref}^2}{2U_\infty^2} \end{bmatrix} \right) \begin{bmatrix} \mathbf{u} \\ \dot{\mathbf{u}} \\ \ddot{\mathbf{u}} \end{bmatrix}.$$

This generalized state-space form with a maximum time derivative term of order 2 for the input vector $\mathbf{u}$ corresponds to a DAE of index 3 [36]. Fig. 1 shows different realizations of the Theodorsen function $C(k)$ in the complex plane for different values of the reduced frequency k, where a comparison with the Jones approximation [37] involving two states is shown. For the Loewner realization the cases corresponding to a number of states equal to that of Jones $(n = 2)$ and eight are depicted. It becomes clear that the Loewner realization for an increasing number of poles is in agreement with the Theodorsen function computed directly in the frequency domain (FD). The number of poles in the Loewner realization is increased by simply modifying the truncation after the SVD decomposition of Eq. 5. Note that unlike for the classical interpolation techniques [38], the Loewner realization does not require the selection of any poles and no iterative optimization is involved. The matrices $\mathbf{A}_c$, $\mathbf{B}_c$, $\mathbf{C}_c$ and $\mathbf{D}_c$ obtained for the case where up to eight states are retained after the SVD decomposition of the Loewner matrix $\mathbb{L}$ are provided in Quero et al. [30].

2.2.2 Sears function

When subjected to a vertical atmospheric gust w_g, the incremental lift coefficient (at the quarter chord position with no additional pitch moment) c_l of the airfoil can be obtained in the frequency domain by means of the Sears function $S(k)$, which depends on the reduced frequency k [39]:

$$S(k) = \frac{2}{\pi k \left(H_0^{(2)}(k) - i H_1^{(2)}(k) \right)}$$

Thus the aerodynamic transfer function matrix for the lift and pitch moment coefficients (c_l and c_m) at the airfoil quarter chord position is:

$$\begin{bmatrix} c_l \\ c_m \end{bmatrix} = \mathbf{H}_s(\omega) w_g,$$

where:

$$\mathbf{H}_s(\omega) = \begin{bmatrix} 2\pi S(k) e^{-ik} \\ 0 \end{bmatrix}.$$

The term $S(k) e^{-ik}$ is commonly referred to as the modified Sears function [40] and its inverse Fourier transform provides the well-known Küssner function [41]. A Loewner realization with 3 and 12 states of the Sears function $S(k)$ is shown in Fig. 2, where a comparison with the three states approximation by Jones [37] is also plotted. There is a very good agreement of the Loewner realization of 12 states with the reference data in the frequency domain (FD). The resulting state-space system in the time domain is:

$$\begin{aligned} \dot{\mathbf{x}}_s &= \mathbf{A}_s \mathbf{x}_s + \frac{2\pi}{U_\infty} \mathbf{B}_s w_g \\ \begin{bmatrix} c_l \\ c_m \end{bmatrix} &= \begin{bmatrix} \mathbf{C}_s \\ \mathbf{0} \end{bmatrix} \mathbf{x}_c. \end{aligned} \tag{8}$$

As in Section 2.2.1, the system $(\mathbf{E}_{sr}, \mathbf{A}_{sr}, \mathbf{B}_{sr}, \mathbf{C}_{sr}, \mathbf{D}_{sr})$ is obtained after applying Eqs. 4 and 6 for a reduction on the number of states and a projection on the Hardy space H_∞, this time on the modified Sears function $S(k) e^{-ik}$. Thus, the matrices:

$$\mathbf{A}_s = \mathbf{E}_{sr}^{-1} \mathbf{A}_{sr},\ \mathbf{B}_s = \mathbf{E}_{sr}^{-1} \mathbf{B}_{sr},\ \mathbf{C}_s = \mathbf{E}_{sr}^{-1} \mathbf{C}_{sr},\ \mathbf{D}_s = \mathbf{E}_{sr}^{-1} \mathbf{D}_{sr} = \mathbf{0}$$

correspond to the realization of the modified Sears function including the complex exponential factor e^{-ik}. In Eq. 8 there is no need for an extended input vector including the time derivative of the gust velocity w_g, as the magnitude of the Sears function tends to zero for increasing reduced frequencies.

3 AEROSERVOELASTIC SYSTEM FOR LOADS ANALYSIS

In this section the Loewner realization (tangential interpolation method) presented in Section 2.1 is applied to the more general case of an aircraft flying in compressible flow. Once the aerodynamic system is described in generalized state-space form in Section 3.1, the structural model is also considered and a coupled aeroservoelastic system for dynamic loads prediction including the FSM method for the cut loads recovery is presented in Section 3.2.

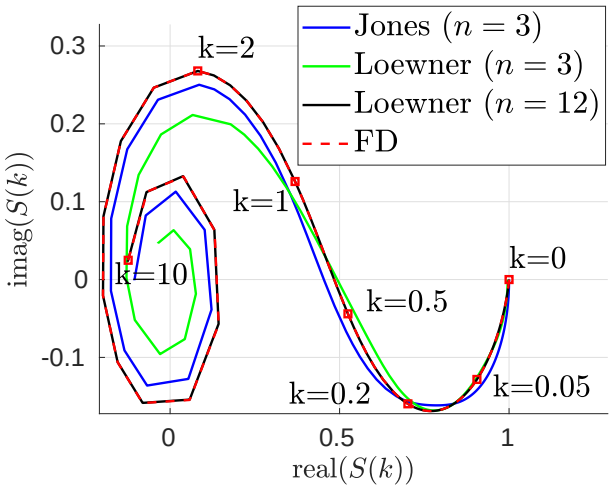

Figure 2: Sears function in the complex plane and corresponding Jones and Loewner approximations.

3.1 Loewner realization of the aerodynamic system

For the general case of three-dimensional unsteady compressible flow the transfer function matrix describing the aerodynamic forces cannot be explicitly obtained as for the bidimensional incompressible case, given by Eq. 7. A common technique for the computation of the subsonic compressible aerodynamic forces for loads application is the doublet lattice method (DLM), which provides the matrix of aerodynamic influence coefficients (AIC) at a set of particular frequencies. Due to the assumption of linear and inviscid flow, the DLM method is not appropriate to describe the transonic flow. In this region other methods such as the correction of the AIC matrices [42] or linearized CFD solvers in the frequency domain can be used [43]. An application including high-fidelity CFD data has been previously shown in Poussot-Vassal et al. [44]. In this work both DLM and high-fidelity linearized CFD methods are considered, see Section 4.

The input of the aerodynamic system is given by the vertical atmospheric disturbance w_g at a particular spatial location (the aircraft nose) and by a set of generalized coordinates corresponding to the control surfaces $\mathbf{u}_c$ and the structural modes $\mathbf{u}_h$ of the aircraft structure (in vacuum) including the rigid-body and flexible modes, as the aeroservoelastic system is reduced by projection on the eigenvalues of the structure (modal truncation). Within the usual assumptions for aeroservoelastic modeling, the translational degrees of freedom $\mathbf{u}_t$ of the aircraft structure do not cause any change in the aerodynamic forces and thus their time derivatives $\dot{\mathbf{u}}_t$ are considered as input to the aerodynamic system. The vector $\mathbf{u}_{rf}$ contains the generalized coordinates corresponding to rotational rigid-body motions and to the flexible modes.

As output of the aerodynamic system the nodal forces and moments splined over the structural grid $\mathbf{P}_{ag}$ by means of the transpose of the spline matrix $\mathbf{H}_{kg}$ for the equivalence of work [45] is chosen:

$$\mathbf{P}_{ag} = \mathbf{H}_{kg}^T \mathbf{P}_{ak}.$$

The vector $\mathbf{P}_{ak}$ represents the aerodynamic contribution to the nodal loads acting on the aerodynamic grid corresponding to the body surface and the spline matrix $\mathbf{H}_{kg}$ transfers the structural

displacements to the aerodynamic grid over the body surface. With the aerodynamic distribution provided by $\mathbf{P}_{ag}$ the cut loads distribution $\mathbf{L}_{FSM}$ can be recovered over the load reference axis (LRA) by means of the FSM. The aerodynamic transfer function matrix of size $N_a \times (N_h + N_c + 1)$ relating the input and output vectors is given in the frequency domain as:

$$\mathbf{P}_{ag}(\omega) = \begin{bmatrix} \mathbf{H}_g(\omega) & \mathbf{H}_t(\omega) & \mathbf{H}_{rf}(\omega) & \mathbf{H}_c(\omega) \end{bmatrix} \begin{bmatrix} w_g(\omega) \\ i\omega \mathbf{u}_t(\omega) \\ \mathbf{u}_{rf}(\omega) \\ \mathbf{u}_c(\omega) \end{bmatrix}, \tag{9}$$

where $\mathbf{H}_t(\omega)) = \mathbf{T}_H \mathbf{H}(\omega)/i\omega$ with $\mathbf{T}_H$ a matrix selecting the columns from $\mathbf{H}(\omega)$ corresponding to the translational degrees of freedom $\mathbf{u}_t$. In this way the singularity caused by the translational motion at frequency zero can be avoided. The number of aerodynamic degrees of freedom is given by N_a and N_h and N_c represent the number of structural modes and control surfaces respectively.

First a realization on the aerodynamic transfer function matrix as provided in Eq. 4 is done. Once the realization $(\hat{\mathbf{E}}, \hat{\mathbf{A}}, \hat{\mathbf{B}}, \hat{\mathbf{C}}, \hat{\mathbf{D}})$ has been obtained the eigenvalues of the system are obtained by solving $\det(s\hat{\mathbf{E}} - \hat{\mathbf{A}}) = 0$. Note that at this stage there is no need for a SVD decomposition of the Loewner matrix as this realization is not the final one representing the aerodynamic system. Similarly, no stabilization by projection into the Hardy space H_∞ is enforced yet. The possible infinite poles due to the non-properness are excluded by setting a tolerance value S_∞ and the remaining finite poles are collected in the set S_f:

$$S_f = \left\{ s \cap \{|s| \leq S_\infty\} \mid \det(s\hat{\mathbf{E}} - \hat{\mathbf{A}}) = 0 \right\}. \tag{10}$$

The column of the aerodynamic transfer function matrix in Eq. 9 corresponding to the gust input $\mathbf{H}_g(\omega)$ is proper and no split into proper and non-proper part is required here. Similarly, no residualization is required when considering the gust disturbance as unique system input [44], as will be shown in Section 4. In order to split the proper and non-proper parts for the rest of the columns of the aerodynamic transfer function matrix $\mathbf{H}(\omega)$ in a numerical stable way, a least-squares fit of a rational proper transfer function together with a polynomial part is done for each component of the transfer function matrix data:

$$H_{ij}(\omega) = \sum_{k=1}^{N_p} \frac{R_{ij}}{i\omega + p_k} + P_{0,ij} + P_{1,ij} i\omega - P_{2,ij} \omega^2, \tag{11}$$

where p_k, R_{ij} can either be real or come in conjugate pairs, $P_{0,ij}, P_{1,ij}, P_{2,ij} \in \mathbb{R}$ and the sum runs over the number N_p of finite poles p_k given by Eq. 10 and which belong to the set S_f defined in Eq. 10, $p_k \in S_f$. Note that compared to the classical least-squares fit of the RFA technique which uses real coefficients [3, 9, 10], Eq. 11 is able represent peaks of the aerodynamic transfer functions in the frequency domain which appear in the transonic flow regime [46] by the presence of conjugate pair poles [5]. Also, the use of a number of poles N_c as done here would lead to a prohibitive number of additional states if the classical approach of a least-squares fit were directly transformed into the time domain [47].

In the next step the actual data after subtraction of the polynomial non-proper part instead of the strictly proper part of the fit given by the first term of Eq. 11 is used. Thus, there is no error introduced in the proper part of the aerodynamic transfer function matrix and the representation of the non-proper part by the polynomial part can be seen as a residualization of the high frequency behaviour of the aerodynamic transfer function matrix $\mathbf{H}(\omega)$.

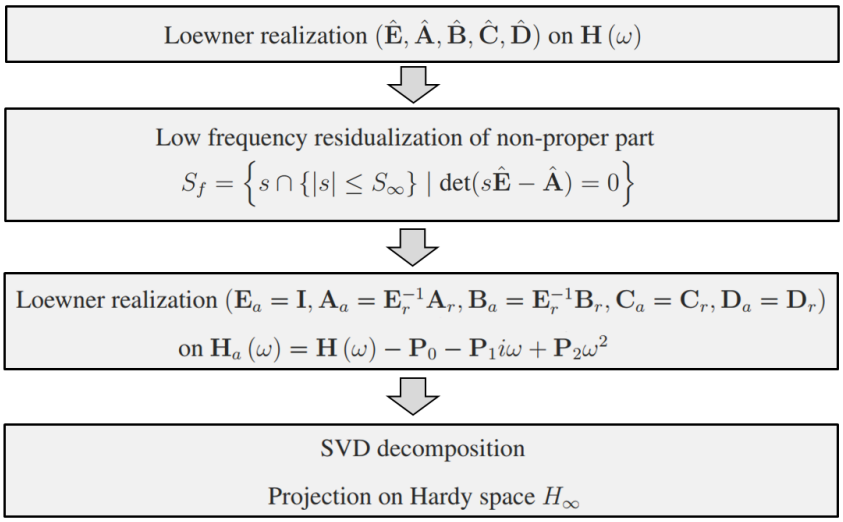

Figure 3: Flow diagram for the Loewner realization of the aerodynamic transfer function matrix considering the proper and non-proper parts.

Next the proper transfer function matrix $\mathbf{H}_a(\omega)$ is obtained, $\mathbf{H}_a(\omega) = \mathbf{H}(\omega) - \mathbf{P}_0 - \mathbf{P}_1 i\omega + \mathbf{P}_2\omega^2$. Similarly as done for the incompressible flow case, now the tangential interpolation method is applied to the proper transfer function matrix $\mathbf{H}_a(\omega)$ and the realization $(\mathbf{E}_a = \mathbf{I}, \mathbf{A}_a = \mathbf{E}_r^{-1}\mathbf{A}_r, \mathbf{B}_a = \mathbf{E}_r^{-1}\mathbf{B}_r, \mathbf{C}_a = \mathbf{C}_r, \mathbf{D}_a = \mathbf{D}_r)$ is obtained, where the SVD decomposition and the projection on the Hardy space H_∞ have been applied. For the sake of clarity, the above described steps are represented in Fig. 3.

The matrices $\mathbf{B}_a$ and $\mathbf{D}_a$ together with the input vector have to be properly completed to accommodate the non-proper polynomial part, see Eq. 12. The matrices corresponding to the polynomial part have been split in column blocks corresponding to the translational motion $(\mathbf{P}_{0t}, \mathbf{P}_{1t}, \mathbf{P}_{2t})$, rotational and flexible generalized coordinates $(\mathbf{P}_{0rf}, \mathbf{P}_{1rf}, \mathbf{P}_{2rf})$ and control surface deflections $(\mathbf{P}_{0c}, \mathbf{P}_{1c}, \mathbf{P}_{2c})$. The term corresponding to the third time derivative of the translational motion $\dddot{\mathbf{u}}_t$ is explicitly neglected by setting $\mathbf{P}_{2t} = 0$ and the submatrices in $[\mathbf{B}_{au1}\ \mathbf{B}_{ah2}\ \mathbf{B}_{ah1}\ \mathbf{B}_{au2}\ \mathbf{0}\ \mathbf{0}\ \mathbf{0}\ \mathbf{0}\ \mathbf{0}\ \mathbf{0}]$ have been defined for convenience in a subsequent reordering of terms.

$$\begin{aligned} \dot{\mathbf{x}_a} &= \mathbf{A}_a\mathbf{x}_a + \left[\begin{array}{cccccccccc} \mathbf{B}_{au1} & \mathbf{B}_{ah2} & \mathbf{B}_{ah1} & \mathbf{B}_{au2} & \mathbf{0} & \mathbf{0} & \mathbf{0} & \mathbf{0} & \mathbf{0} & \mathbf{0} \end{array}\right]\mathbf{u}_a \\ \mathbf{P}_{ag} &= \mathbf{C}_a\mathbf{x}_a + \left[\begin{array}{cccccccccc} \mathbf{0} & \mathbf{P}_{0t} & \mathbf{P}_{0rf} & \mathbf{P}_{0c} & \mathbf{P}_{1t} & \mathbf{P}_{1rf} & \mathbf{P}_{1c} & \mathbf{0} & -\mathbf{P}_{2rf} & -\mathbf{P}_{2c} \end{array}\right]\mathbf{u}_a, \end{aligned} \tag{12}$$

where $\mathbf{u}_a = [w_g\ \dot{\mathbf{u}}_t^T\ \mathbf{u}_{rf}^T\ \mathbf{u}_c^T\ \ddot{\mathbf{u}}_t^T\ \dot{\mathbf{u}}_{rf}^T\ \dot{\mathbf{u}}_c^T\ \dddot{\mathbf{u}}_t^T\ \ddot{\mathbf{u}}_{rf}^T\ \ddot{\mathbf{u}}_c^T]^T$. Dropping the terms corresponding to zero submatrices and reordering, the generalized state-space model for the unsteady aerodynamic loads is:

$$\begin{aligned} \dot{\mathbf{x}}_a &= \mathbf{A}_a\mathbf{x}_a + \left[\begin{array}{cccc} \mathbf{B}_{au1} & \mathbf{B}_{au2} & \mathbf{0} & \mathbf{0} \end{array}\right]\left[\begin{array}{c} w_g \\ \mathbf{u}_c \\ \dot{\mathbf{u}}_c \\ \ddot{\mathbf{u}}_c \end{array}\right] + \left[\begin{array}{cc} \mathbf{B}_{ah1} & \mathbf{B}_{ah2} \end{array}\right]\left[\begin{array}{c} \mathbf{u}_{rf} \\ \dot{\mathbf{u}}_t \end{array}\right] \\ \mathbf{P}_{ag} &= \mathbf{C}_a\mathbf{x}_a + \left[\begin{array}{cccc} \mathbf{0} & \mathbf{P}_{0c} & \mathbf{P}_{1c} & -\mathbf{P}_{2c} \end{array}\right]\left[\begin{array}{c} w_g \\ \mathbf{u}_c \\ \dot{\mathbf{u}}_c \\ \ddot{\mathbf{u}}_c \end{array}\right] + \left[\begin{array}{ccc} \mathbf{P}_{0rf} & \mathbf{D}_{ah2} & \mathbf{D}_{ah3} \end{array}\right]\left[\begin{array}{c} \mathbf{u}_{rf} \\ \dot{\mathbf{u}}_h \\ \ddot{\mathbf{u}}_h \end{array}\right], \end{aligned} \tag{13}$$

where $\mathbf{u}_h = [\mathbf{u}_t^T \ \mathbf{u}_{rf}^T]^T$ and:

$$\mathbf{D}_{ah2} = \begin{bmatrix} \mathbf{P}_{0t} & \mathbf{P}_{1rf} \end{bmatrix}$$
$$\mathbf{D}_{ah3} = \begin{bmatrix} \mathbf{P}_{1t} & -\mathbf{P}_{2rf} \end{bmatrix}$$

Note that some other approaches neglect the low frequency residualization of the non-proper part of the transfer function matrix by neglecting the high frequency content instead. For instance, Fonte [23] considers the loads only up to a defined frequency value, introducing a low-pass filter with high bandwidth. In principle the time delay introduced by the casual filter would have then to be taken into consideration.

3.2 Aeroservoelastic system

In this section the interaction between the aerodynamic and structural parts are considered in order to obtain a complete aeroservoelastic formulation. As in Section 3.1, the transfer of the aerodynamic forces to the structural grid is done by the spline matrix $\mathbf{H}_{kg}^T$. The aeroservoelastic problem can be formulated in the time domain as:

$$\begin{aligned}&\mathbf{M}_{hh}\ddot{\mathbf{u}}_h + \mathbf{B}_{hh}\dot{\mathbf{u}}_h + \mathbf{K}_{hh}\mathbf{u}_h \\ =&\boldsymbol{\phi}_{gh}^T \left(\mathbf{C}_a\mathbf{x}_a + \begin{bmatrix} \mathbf{0} & \mathbf{P}_{0c} & \mathbf{P}_{1c} & -\mathbf{P}_{2c} \end{bmatrix} \begin{bmatrix} w_g \\ \mathbf{u}_c \\ \dot{\mathbf{u}}_c \\ \ddot{\mathbf{u}}_c \end{bmatrix} + \begin{bmatrix} \mathbf{P}_{0rf} & \mathbf{D}_{ah2} & \mathbf{D}_{ah3} \end{bmatrix} \begin{bmatrix} \mathbf{u}_{rf} \\ \dot{\mathbf{u}}_h \\ \ddot{\mathbf{u}}_h \end{bmatrix} \right),\end{aligned}$$

where $\mathbf{M}_{hh}$, $\mathbf{B}_{hh}$ and $\mathbf{K}_{hh}$ represent the generalized mass, damping and stiffness matrices respectively. The matrix $\boldsymbol{\phi}_{gh}$ contains a number N_h (due to modal truncation) of the aircraft structural modes $\mathbf{u}_h$ (in vacuum) including the rigid-body and flexible modes. As in Section 3.1, the vector $\mathbf{u}_h = [\mathbf{u}_t^T \ \mathbf{u}_{rf}^T]^T$ represents the total number of generalized coordinates (including rigid-body and structural flexible modes) and $\mathbf{u}_c$ the control surfaces. The subset $\mathbf{u}_t \subset \mathbf{u}_h$ represents the translational rigid-body degrees of freedom and the subset $\mathbf{u}_{rf} \subset \mathbf{u}_h$ the rotational rigid-body degrees of freedom together with the flexible modes.

In order to include the translational motion in the system output, the state vector $\mathbf{x}$ is augmented, $\hat{\mathbf{x}} = [\mathbf{u}_t^T \ \mathbf{u}_{rf}^T \ \dot{\mathbf{u}}_h^T \ \mathbf{x}_a^T]^T$, and the following equation of first order in the time derivatives is obtained:

$$\begin{aligned}\frac{d}{dt}\left(\begin{bmatrix} \mathbf{u}_t \\ \mathbf{u}_{rf} \\ \dot{\mathbf{u}}_h \\ \mathbf{x}_a \end{bmatrix} \right) &= \begin{bmatrix} \mathbf{0} & \mathbf{0} & \mathbf{T}_t & \mathbf{0} \\ \mathbf{0} & \mathbf{0} & \mathbf{T}_{rf} & \mathbf{0} \\ \mathbf{0} & \mathbf{A}_{h1} & \mathbf{A}_{h2} & \mathbf{A}_{h3} \\ \mathbf{0} & \mathbf{B}_{ah1} & \mathbf{B}_{ah2}\mathbf{T}_t & \mathbf{A}_a \end{bmatrix} \begin{bmatrix} \mathbf{u}_t \\ \mathbf{u}_{rf} \\ \dot{\mathbf{u}}_h \\ \mathbf{x}_a \end{bmatrix} \\ &+ \begin{bmatrix} \mathbf{0} & \mathbf{0} & \mathbf{0} & \mathbf{0} \\ \mathbf{0} & \mathbf{0} & \mathbf{0} & \mathbf{0} \\ \mathbf{0} & \boldsymbol{\alpha}^{-1}\boldsymbol{\phi}_{gh}^T\mathbf{P}_{0c} & \boldsymbol{\alpha}^{-1}\boldsymbol{\phi}_{gh}^T\mathbf{P}_{1c} & -\boldsymbol{\alpha}^{-1}\boldsymbol{\phi}_{gh}^T\mathbf{P}_{2c} \\ \mathbf{B}_{au1} & \mathbf{B}_{au2} & \mathbf{0} & \mathbf{0} \end{bmatrix} \begin{bmatrix} w_g \\ \mathbf{u}_c \\ \dot{\mathbf{u}}_c \\ \ddot{\mathbf{u}}_c \end{bmatrix},\end{aligned} \tag{14}$$

with:

$$
\begin{aligned}
\boldsymbol{\alpha} &= \mathbf{M}_{hh} - \boldsymbol{\phi}_{gh}^T \mathbf{D}_{ah3} \\
\mathbf{A}_{h1} &= \boldsymbol{\alpha}^{-1} \left(-\mathbf{k}_{hf} \mathbf{T}_f + \boldsymbol{\phi}_{gh}^T \mathbf{P}_{0rf} \right) \\
\mathbf{A}_{h2} &= \boldsymbol{\alpha}^{-1} \left(-\mathbf{B}_{hh} + \boldsymbol{\phi}_{gh}^T \mathbf{D}_{ah2} \right) \\
\mathbf{A}_{h3} &= \boldsymbol{\alpha}^{-1} \boldsymbol{\phi}_{gh}^T \mathbf{C}_a .
\end{aligned}
$$

The matrix $\mathbf{T}_{rf}$ selects the non translational degrees of freedom $\mathbf{u}_{rf}$ from the generalized coordinates $\mathbf{u}_h$ (that is, excluding the subset $\mathbf{u}_t$ corresponding to the translational motion) and the matrix $\mathbf{T}_t$ selects the translational degrees of freedom from the vector of generalized coordinates $\mathbf{u}_h$.

Once the aeroelastic system has been written in a generalized state-space form the loads can be recovered by the equilibrium of forces (FSM) [48]:

$$
\mathbf{L}_{FSM} = \mathbf{T}_{cg} \left(-\mathbf{M}_{gg} \boldsymbol{\phi}_{gh} \ddot{\mathbf{u}}_h + \mathbf{P}_{ag} \right) ,
$$

where the matrix $\mathbf{M}_{gg}$ represents the physical mass matrix and the summation matrix $\mathbf{T}_{cg}$ sums up the nodal forces and moments acting to the cut loads distribution at the LRA locations. Note that unlike for the MDM method, the FSM method requires not only the generalized aerodynamic forces $\boldsymbol{\phi}_{gh}^T \mathbf{P}_{ag}$ but also the aerodynamic distribution $\mathbf{P}_{ag}$. In Eq. 15 the FSM method has been included in the output of the aeroservoelastic system:

$$
\begin{bmatrix} \mathbf{u}_t \\ \mathbf{u}_{rf} \\ \mathbf{P}_{ag} \\ \mathbf{L}_{FSM} \end{bmatrix} = \begin{bmatrix} \mathbf{I} & \mathbf{0} & \mathbf{0} & \mathbf{0} \\ \mathbf{0} & \mathbf{I} & \mathbf{0} & \mathbf{0} \\ \mathbf{0} & \mathbf{P}_{0rf} + \mathbf{D}_{ah3} \mathbf{A}_{h1} & \mathbf{D}_{ah2} + \mathbf{D}_{ah3} \mathbf{A}_{h2} & \mathbf{C}_a + \mathbf{D}_{ah3} \mathbf{A}_{h3} \\ \mathbf{0} & \mathbf{T}_{cg} \mathbf{P}_{0rf} + \boldsymbol{\beta} \mathbf{A}_{h1} & \mathbf{T}_{cg} \mathbf{D}_{ah2} + \boldsymbol{\beta} \mathbf{A}_{h2} & \mathbf{T}_{cg} \mathbf{C}_a + \boldsymbol{\beta} \mathbf{A}_{h3} \end{bmatrix} \begin{bmatrix} \mathbf{u}_t \\ \mathbf{u}_{rf} \\ \dot{\mathbf{u}}_h \\ \mathbf{x}_a \end{bmatrix}
$$

$$
+ \begin{bmatrix} \mathbf{0} & \mathbf{0} & \mathbf{0} & \mathbf{0} \\ \mathbf{0} & \mathbf{0} & \mathbf{0} & \mathbf{0} \\ \mathbf{0} & \mathbf{P}_{0c} + \mathbf{D}_{ah3} \boldsymbol{\alpha}^{-1} \boldsymbol{\phi}_{gh}^T \mathbf{P}_{0c} & \mathbf{P}_{1c} + \mathbf{D}_{ah3} \boldsymbol{\alpha}^{-1} \boldsymbol{\phi}_{gh}^T \mathbf{P}_{1c} & -\left(\mathbf{P}_{2c} + \mathbf{D}_{ah3} \boldsymbol{\alpha}^{-1} \boldsymbol{\phi}_{gh}^T \mathbf{P}_{2c} \right) \\ \mathbf{0} & \boldsymbol{\Gamma} \mathbf{P}_{0c} & \boldsymbol{\Gamma} \mathbf{P}_{1c} & -\boldsymbol{\Gamma} \mathbf{P}_{2c} \end{bmatrix} \begin{bmatrix} w_g \\ \mathbf{u}_c \\ \dot{\mathbf{u}}_c \\ \ddot{\mathbf{u}}_c \end{bmatrix} , \tag{15}
$$

where:

$$
\begin{aligned}
\boldsymbol{\beta} &= -\mathbf{T}_{cg} \mathbf{M}_{gg} \boldsymbol{\phi}_{gh} + \mathbf{T}_{cg} \mathbf{D}_{ah3} \\
\boldsymbol{\Gamma} &= \boldsymbol{\beta} \boldsymbol{\alpha}^{-1} \boldsymbol{\phi}_{gh}^T + \mathbf{T}_{cg} .
\end{aligned}
$$

Eqs. 14 and 15 represent the generalized state-space and output equations for the aeroservoelastic model description in the time domain and Fig. 4 depicts the corresponding aeroservoelastic system including the cut loads obtained by the FSM. There, the matrix $\mathbf{T}_h$ selects the subset $\mathbf{u}_h$ from the vector $[w_g \ \mathbf{u}_c^T \ \mathbf{u}_h^T]^T$.

4 APPLICATION TO THE NASA COMMON RESEARCH MODEL CONFIGURATION

In this section the structural FERMAT model as created by Klimmek [49] for the NASA CRM configuration [50] has been used. The mass case C2 corresponding to a 100 % of the fuel mass with a mass equal to the maximum takeoff weight MTOW $= 260000$ (kg) and a center of gravity position in x direction (see Fig. 5 for axes definition) with respect to the aircraft nose

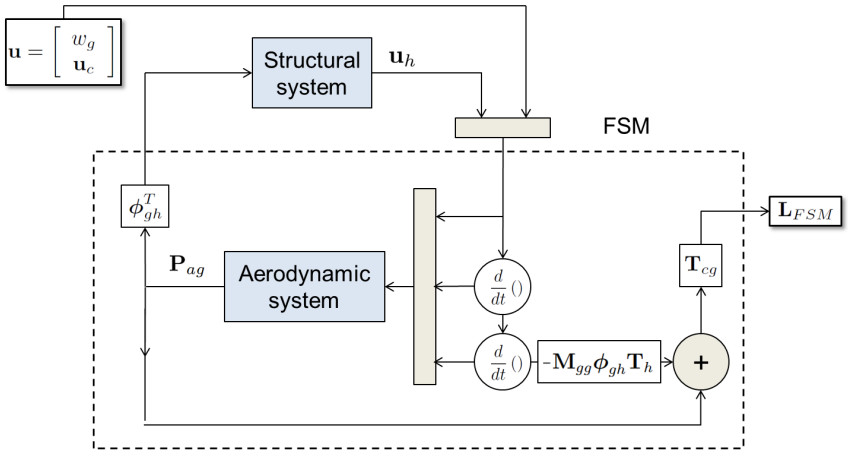

Figure 4: Aeroservoelastic system with the force summation method (FSM) for the cut loads recovery.

position x_0 of $x_{cg} - x_0 = 33.714$ (m) is considered. For the DLM case both open-loop and closed-loop configurations after the synthesis of an H_∞-optimal controller are presented. Note that the cut loads presented in this section are incremental and do not include the loads acting at the 1g or level flight condition.

The aeroservoelastic system as described in Section 3.2 has been generated for the flightpoint corresponding to a Mach number of $M_\infty = 0.86$ and an altitude $h = 9100$ (m). The true airspeed is $U_\infty = 260.892$ (m/s) and the reference length for the reduced frequency definition $L_{ref} = 7$ (m). In Section 4.1 the aerodynamic loads as obtained by the DLM method are used, whereas in Section 4.2 the high-fidelity linearized Reynolds-averaged Navier-Stokes (RANS) equations are considered.

4.1 DLM

As stated in Section 3.2, the spline from the structural model deformation to the aerodynamic grid is carried out by by the transpose of the spline matrix corresponding to a nearest-neighbour force mapping. Neglecting the aerodynamic modeling of the fuselage component there are a total of 1910 aerodynamic panels representing the complete configuration. The wing semi-span is $b/2 = 29.38$ (m). A view of the right wing component is provided in Fig. 5. Note that a strip can include panels from the wing component as well as from the aileron if they are topologically connected. The ailerons are taken into account in Section 4.1.2, where the effect of a gust loads alleviation (GLA) strategy is evaluated using the proposed aeroservoelastic model. In that case, the control surface modes corresponding to the ailerons are modeled with the transpiration approach as described in Section 3.1.

Regarding the dynamic structural model, two symmetric rigid-body modes corresponding to the heave and pitch (around the center of gravity) motion together with the first symmetric wing bending mode have been taken into account. The heave forms the vector $\mathbf{u}_t$ and the pitch together with the first symmetric mode form the vector $\mathbf{u}_{rf}$ in Eq. 15. The interpolation of the precomputed AIC matrices to the set of reduced frequencies selected for the Loewner realization is done using a special linear interpolation [51]. The tolerance in Eq. 10 has been set to $S_\infty = 10\,(U_\infty/L_{ref})$.

Fig. 6 shows the element of the aerodynamic transfer function matrix corresponding to the incremental lift coefficient over the strip element at the wing station $y = 13.48$ (m) in the

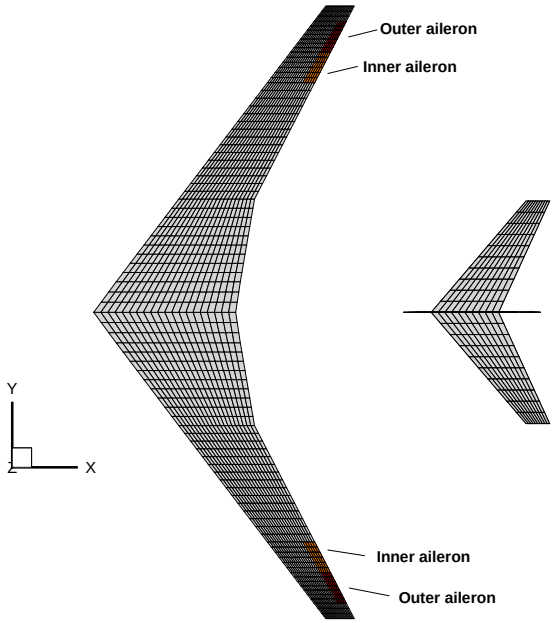

Figure 5: DLM panels and corresponding control surfaces (red and orange) for the NASA CRM configuration.

complex plane due to a gust disturbance input for the different values of the reduced frequency k. In Fig. 7 the pitch motion around the center of gravity is taken as input. For comparison purposes the results obtained with six real poles applying the classical Roger's approach (RFA) is also shown. The data labeled as Loewner shows the present method and FD refers to the reference data in the frequency domain. It is clear from Figs. 6 and 7 that the present approach shows a better match compared to the Roger's approach. Because of the finer resolution for the low reduced frequency range in the set of reduced frequencies selected, this better match is more evident in this region which is of significant importance for aeroelastic applications.

4.1.1 Open-loop

Two different aeroservoelastic models are generated. Both contain two symmetric rigid-body modes corresponding to the heave and pitch motions but differ in the number of symmetric flexible modes considered. The first one includes the first flexible mode corresponding to the wing bending with a natural frequency of 1.0574 (Hz) resulting in a total of 96 states and the second one includes 16 symmetric flexible modes contained in a frequency interval which ranges up to a value of 16.3742 (Hz) with a total number of 231 states. These time-domain aeroservoelastic modes are validated in open-loop against the reference aeroelastic model available in the frequency domain. For the validation, the system is excited with a *1-cosine* gust $w_g\,(t)$ in (m/s) given by (at the aircraft nose) [1] of amplitude w_0 (m/s), translational speed U_∞ (m/s) and half length H (m). For this application the gust amplitude has been set to $\alpha_{eq} = w_0/U_\infty$ equivalent to 1 (deg) and two different gust gradient values of $H = 50$ and $H = 350$ (ft) are considered.

The corresponding incremental bending $\triangle MX$ and torsional $\triangle MY$ moments obtained by the FSM over the right wing component as predicted by both the aeroservoelastic model in the time domain (labeled as TD) and the reference model in the frequency domain (labeled as FD) for a gust gradient $H = 50$ (ft) are shown in Figs. 8 and 9 for the time instants at which the maximum and minimum vales are reached at the wing root location. In Fig. 8 one flexible modes are considered, whereas in Fig. 9 the model with 16 flexible modes is shown. As specified above,

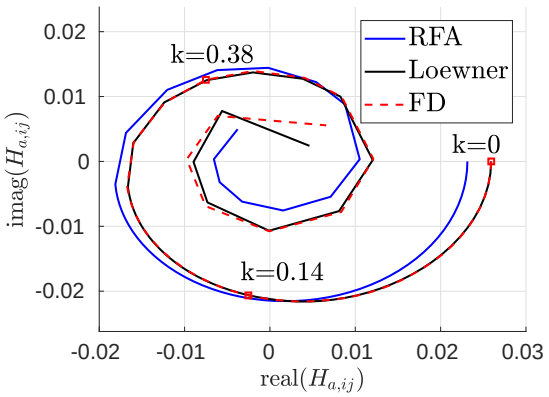

Figure 6: Element of the transfer function matrix from the gust input to the lift coefficient for the strip at wing station $y = 13.48$ (m).

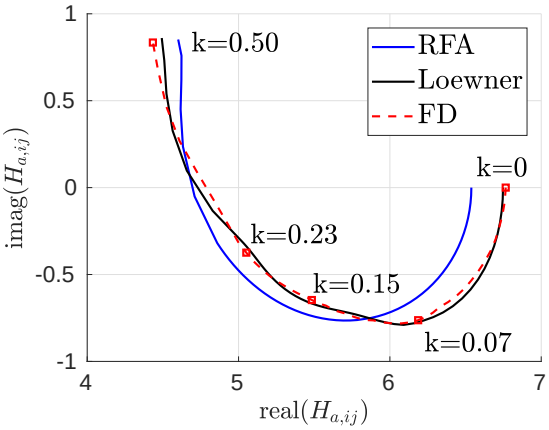

Figure 7: Element of the transfer function matrix from the pitch input to the lift coefficient for the strip at wing station $y = 13.48$ (m).

both include two symmetric rigid-body modes. In both cases the aeroservoelastic model is able to reproduce the complete time history of the incremental cut loads distribution along the entire wing component.

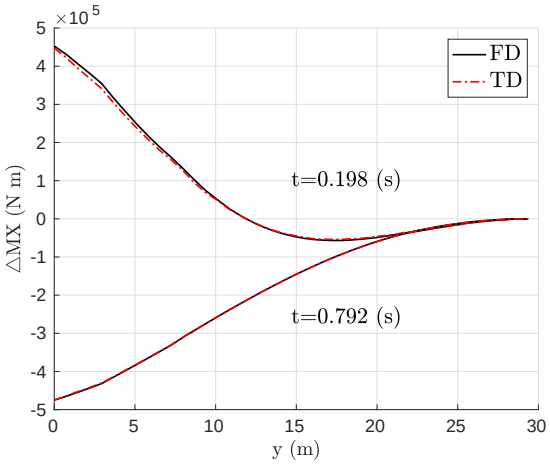

Figure 8: Incremental bending moment $\triangle MX$ over the right wing component at different time instants for $M_\infty = 0.86$, $h = 9100$ (m), $H = 50$ (ft), $\alpha_{eq} = 1$ (deg). Results obtained in the frequency domain (FD) and with the generalized state-space model in the time domain (TD) by the FSM with one flexible mode. The number of states is 96.

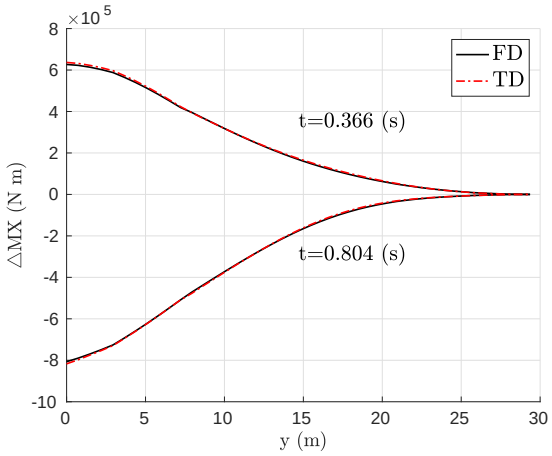

Figure 9: Incremental bending moment $\triangle MX$ over the right wing component at different time instants for $M_\infty = 0.86$, $h = 9100$ (m), $H = 50$ (ft), $\alpha_{eq} = 1$ (deg). Results obtained in the frequency domain (FD) and with the generalized state-space model in the time domain (TD) by the FSM with 16 flexible modes. The number of states is 231.

In Figs. 10 and 11 the corresponding results for a gust gradient value of $H = 350$ (ft) are presented. Again, the aeroservoelastic model is able to reproduce the reference results in the frequency domain (FD).

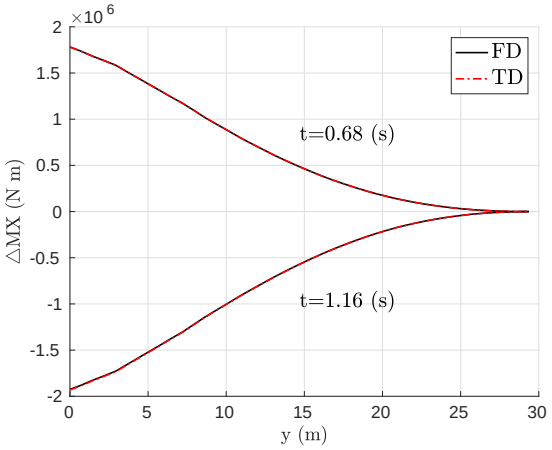

Figure 10: Incremental bending moment $\triangle MX$ over the right wing component at different time instants for $M_\infty = 0.86$, $h = 9100$ (m), $H = 350$ (ft), $\alpha_{eq} = 1$ (deg). Results obtained in the frequency domain (FD) and with the generalized state-space model in the time domain (TD) by the FSM with one flexible mode. The number of states is 96.

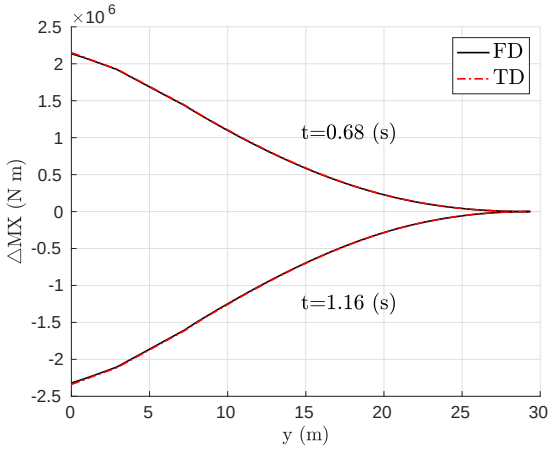

Figure 11: Incremental bending moment $\triangle MX$ over the right wing component at different time instants for $M_\infty = 0.86$, $h = 9100$ (m), $H = 350$ (ft), $\alpha_{eq} = 1$ (deg). Results obtained in the frequency domain (FD) and with the generalized state-space model in the time domain (TD) by the FSM with 16 flexible modes. The number of states is 231.

4.1.2 Closed-loop

Once the aeroservoelastic model has been validated in open-loop, the implementation of a GLA strategy is shown. Here an H_∞-optimal strategy for the controller synthesis [52, 53] including the two rigid-body modes and the first flexible mode has been considered. The name H_∞ makes reference to the Hardy space H_∞ where the optimization takes place. The order of the controller is $N_K = 7$ and all controller parameters are set to free for the optimization problem. Additionally, a loop-shaping by means of weighting performances has been applied [52]. The H_∞ controller synthesis is possible due to the generation of the complete aeroservoelastic model with a number of states in the order of hundreds, which is an acceptable size for the open-loop system [53]. The objective is to minimize the incremental bending moment at the wing root position by means of a symmetric deflection of the outer ailerons.

As discussed in Section 3, the application of the FSM for the cut loads recovery results in a non-proper part of the corresponding transfer function components. In this work the weight performances applied to the H_∞ controller synthesis consider the transfer function up to a certain frequency value and thus neglect the high frequency behaviour for the optimization problem to be solved for the controller design. For an extension including the non-proper part of the transfer function caused by the time derivative of the aileron input see Poussot-Vassal et al. [54].

In this case the first model of Section 4.1.1 including two symmetric rigid-body modes and one flexible mode has been considered. The selected flightpoint remains unchanged and a corresponding H_∞-optimal controller is designed. The aeroelastic response to a gust input of amplitude $\alpha_{eq} = 1$ (deg) and gust gradient $H = 350$ (ft) has been considered next. For this specific gust input, the maximum outer aileron deflection produced by the controller is 1.93

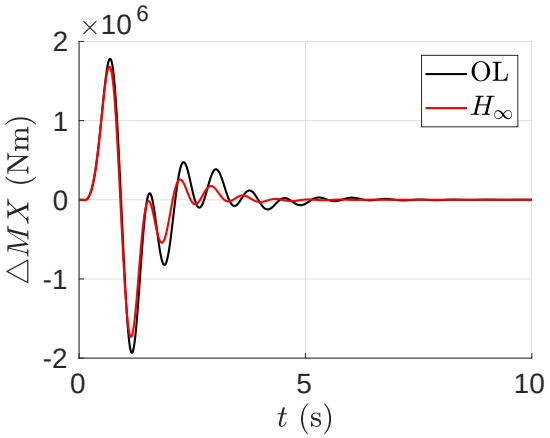

Figure 12: Time history of the incremental bending moment $\triangle MX$ at the wing root with and without GLA strategy.

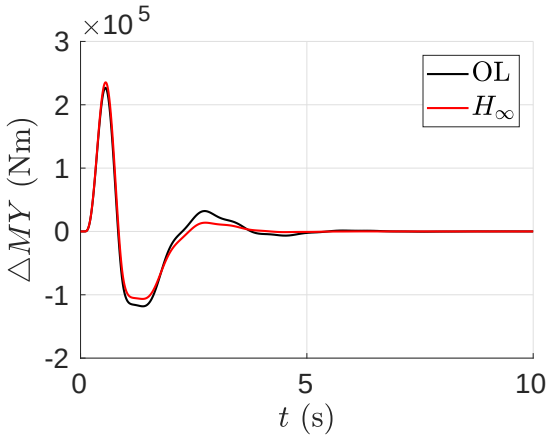

Figure 13: Time history of the incremental torsional moment $\triangle MY$ at the wing root with and without GLA strategy.

(deg). In Fig. 12 the incremental wing root bending moment is shown as a function of time for both the open-loop (OL) and the closed-loop (H_∞) cases. By deploying the outer ailerons in a symmetric way, the controller is able to reduce the maximum value of the incremental wing root bending moment caused by the gust $\triangle MX$ in 5.6 % for the maximum peak and in 10.4 % for the minimum peak at the expense of increasing the incremental torsional moment $\triangle MY$ in 3.8 % for its maximum peak value, see Fig. 13. Further, the proposed aeroservoelastic model enables the evaluation of the effects of the applied GLA strategy on the cut loads over the complete aircraft structure.

4.2 High-fidelity CFD

The aerodynamic half-model used for the high-fidelity computations is based on the publicly available grid from the 4th AIAA Drag Prediction Workshop [50] and includes the wing, horizontal tail plane and fuselage components. The hybrid unstructured and structured volume mesh contains around 3.7 million points, of which 1000014 are located over the component surface. The farfield boundary is a semisphere with a radius of 757 (m).

The aerodynamic shape corresponds to a cruise flight condition with a global lift coefficient of $C_L = 0.5$ at a Mach number of $M_\infty = 0.86$, an altitude of $h = 9100$ (m) and a steady angle of attack $\alpha_0 = 1.641$ (deg). The corresponding steady pressure coefficient distribution c_p is shown in Fig. 14, where a recompression shock wave is present at the upper wing surface. However, the flow remains fully attached.

For the high-fidelity unsteady aerodynamic response the linear frequency domain (LFD) solver for the RANS equations of the DLR TAU-Code has been chosen [43, 55]. The aircraft is considered rigid and thus only the aerodynamic contribution without the aeroelastic response is considered, which is equivalent to setting all the terms to zero in the state-space vector except for $\mathbf{x}_a$ in Eqs. 14 and 15.

The same gust input with $H = 350$ (ft) as in Section 4.1.2 is considered. When considering the high-fidelity modeling of the aerodynamic forces, a higher number of states are required in the Loewner realization when compared to the aerodynamic forces predicted by the DLM

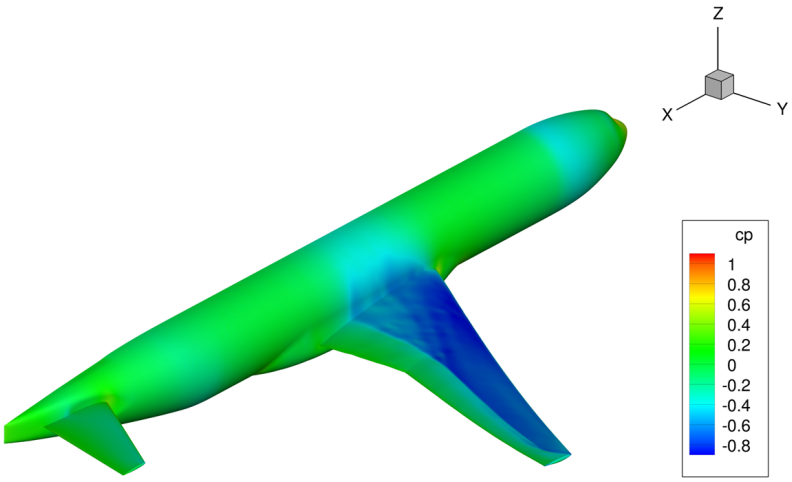

Figure 14: Steady pressure coefficient distribution c_p for $M_\infty = 0.86$, $h = 9100$ (m) and $\alpha_0 = 1.641$ (deg). NASA CRM model.

potential method from Section 4.1. In this case a total number of states of 300 has been selected, which is shown to properly reproduce the reference results in the frequency domain (FD) as produced by the LFD solver in the complex plane, see Fig. 15, where the aerodynamic transfer function matrix for a node at position $x = 30.1076$ (m), $y = 3.6521$ (m), $z = 3.9362$ (m) is depicted. In Fig. 16 the incremental bending moment along the wing right component for the time values at which the maximum and minimum values at the wing root location are reached are shown. Again, the time-domain aerodynamic model (TD) is able to represent the complete cut loads distribution along the wing component when compared with the reference results in the frequency domain (FD).

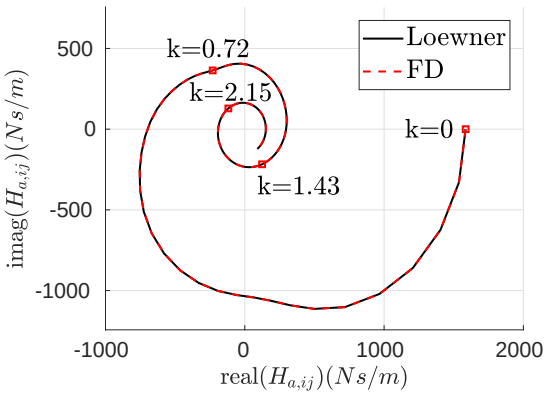

Figure 15: Element of the aerodynamic transfer function matrix from the gust input to the the vertical force for a node at position $x = 30.1076$ (m), $y = 3.6521$ (m), $z = 3.9362$ (m).

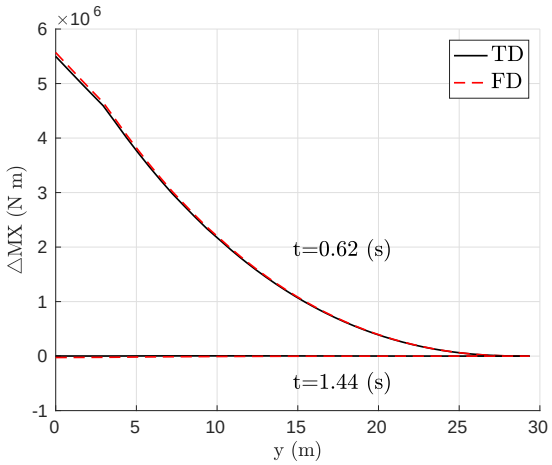

Figure 16: Incremental bending moment $\triangle MX$ over the right wing component at different time instants for $M_\infty = 0.86$, $h = 9100$ (m), $\alpha_0 = 1.641$ (deg), $H = 350$ (ft), $\alpha_{eq} = 1$ (deg). Results obtained by LFD in the frequency domain (FD) and with the generalized state-space model in the time domain (TD) for a rigid aircraft. The number of states is 300.

5 CONCLUSIONS

In this work an aeroservoelastic model for the prediction of the aeroelastic response together with the dynamic loads distribution over the complete aircraft structure has been presented. It represents an interpolation instead of an approximation of the reference model in the frequency domain and avoids any selection of poles as for the classical methods. Thus, the aerodynamic forces distribution caused by the gust disturbance and induced by the aircraft motion can be properly described in the time domain. Once the aerodynamic model has been obtained in the time domain the structural model is taken into account and an aeroservoelastic state-space model of first order in time which includes the effect of control surfaces deflection has been derived.

Aerodynamic forces obtained in the frequency domain from solvers with different fidelity levels have been considered for the NASA CRM / FERMAT configuration, showing that the number of states required for a proper representation of the aerodynamic model increases with the level of complexity. Additionally, the design of a H_∞-optimal controller with the generated aeroservoelastic framework has been demonstrated, while at the same time the presented model is able to assess the cut loads distribution over the complete aircraft.

Related future work includes:

- Generation of a complete aeroservoelastic framework for high-fidelity aerodynamic methods, as presented in this work for the case of DLM solvers.
- Application of the developed framework to flutter stability analysis.
- Inclusion of parametric generalized state-space aeroservoelastic models as an alternative to the classical gain scheduling approach [56].
- Extension to nonlinear generalized state-space formulation of a nonlinear aeroservoelastic system. In this case the Loewner framework in connection with a functional or Volterra series expansion theory can be followed [57].

ACKNOWLEDGMENTS

This work has been funded within the frame of the Joint Technology Initiative JTI Clean Sky 2, AIRFRAME Integrated Technology Demonstrator platform AIRFRAME ITD (contract N. CSJU-CS2-GAM-AIR-2014-15-01 Annex 1, Issue B04, October 2nd, 2015) being part of the Horizon 2020 research and Innovation framework program of the European Commission.

6 REFERENCES

[1] European Aviation Safety Agency (2015). Certification specifications and acceptable means of compliance for large aeroplanes, CS-25, Amendment 16. Tech. rep.

[2] Aviation, Risingup (2015). Federal aviation regulations part 25: Airworthiness standards: Transport category airplanes. *Web resource for research:* `http://www.risingup.com/fars/info/25-index.shtml`.

[3] Roger, K. L. (1977). Airplane math modeling methods for active control design. *AGARD-CP-228*, 4.1–4.11.

[4] Abel, I. (1979). An analytical technique for predicting the characteristics of a flexible wing equipped with an active flutter-suppression system and comparison with wind-tunnel data. Tech. rep., NASA Technical Paper 1367.

[5] Gustavsen, B. and Semlyen, A. (1999). Rational approximation of frequency domain responses by vector fitting. *IEEE Transactions on power delivery*, 14(3), 1052–1061. http://dx.doi.org/10.1109/61.772353.

[6] Gustavsen, B. and Semlyen, A. (2004). A robust approach for system identification in the frequency domain. *IEEE Transactions on Power Delivery*, 19(3), 1167–1173. http://dx.doi.org/10.1109/TPWRD.2003.822530.

[7] Dunn, H. (1980). An analytical technique for approximating unsteady aerodynamics in the time domain. Tech. rep., NASA Technical Paper 1738.

[8] Tiffany, S. and Adams Jr., W. (1987). Nonlinear programming extensions to rational function approximations of unsteady aerodynamics. In *28th Structures, Structural Dynamics and Materials Conference*.

[9] Karpel, M. (1982). Design for active flutter suppression and gust alleviation using state-space aeroelastic modeling. *Journal of Aircraft*, 19(3), 221–227. https://doi.org/10.2514/3.57379.

[10] Eversman, W. and Tewari, A. (1991). Consistent rational-function approximation for unsteady aerodynamics. *Journal of Aircraft*, 28(9), 545–552. https://doi.org/10.2514/3.46062.

[11] Pototzky, A. and Perry III, B. (1986). New and existing techniques for dynamic loads analyses of flexible airplanes. *Journal of Aircraft*, 23(4), 340–347. https://doi.org/10.2514/3.45309.

[12] Karpel, M. and Presente, E. (1995). Structural dynamic loads in response to impulsive excitation. *Journal of Aircraft*, 32(4), 853–861. https://doi.org/10.2514/3.46801.

[13] Haghighat, S., Liu, H., and Martins, J. (2012). Model-predictive gust load alleviation controller for a highly flexible aircraft. *Journal of Guidance, Control, and Dynamics*, 35(6), 1751–1766. doi:10.2514/1.57013. https://doi.org/10.2514/1.57013.

[14] Liu, X., Sun, Q., and Cooper, J. (2017). LQG based model predictive control for gust load alleviation. *Aerospace Science and Technology*, 71, 499–509. https://doi.org/10.1016/j.ast.2017.10.006.

[15] Juang, J. and Pappa, R. (1985). An eigensystem realization algorithm for modal parameter identification and model reduction. *Journal of Guidance, Control, and Dynamics*, 8(5), 620–627. https://doi.org/10.2514/3.20031.

[16] Silva, W. and Bartels, R. (2004). Development of reduced-order models for aeroelastic analysis and flutter prediction using the CFL3Dv6.0 code. *Journal of Fluids and Structures*, 19(6), 729–745. https://doi.org/10.1016/j.jfluidstructs.2004.03.004.

[17] Gaitonde, A. and Jones, D. (2003). Reduced order state-space models from the pulse responses of a linearized CFD scheme. *International journal for numerical methods in fluids*, 42(6), 581–606. https://doi.org/10.1002/fld.527.

[18] Kramer, B. and Gugercin, S. (2016). Tangential interpolation-based eigensystem realization algorithm for MIMO systems. *Mathematical and Computer Modelling of Dynamical Systems*, 22(4), 282–306. https://doi.org/10.1080/13873954.2016.1198389.

[19] Mayo, A. and Antoulas, A. (2007). A framework for the solution of the generalized realization problem. *Linear algebra and its applications*, 425(2-3), 634–662. https://doi.org/10.1016/j.laa.2007.03.008.

[20] Antoulas, A. (2005). *Approximation of large-scale dynamical systems*, vol. 6. Siam.

[21] Brunton, S. L., Dawson, S., and Rowley, C. (2014). State-space model identification and feedback control of unsteady aerodynamic forces. *Journal of Fluids and Structures*, 50, 253–270. https://doi.org/10.1016/j.jfluidstructs.2014.06.026.

[22] Zhao, Y., Yue, C., and Hu, H. (2016). Gust load alleviation on a large transport airplane. *Journal of Aircraft*, 53(6), 1932–1946. doi:10.2514/1.C033713. https://doi.org/10.2514/1.C033713.

[23] Fonte, F. (2018). *Design and validation of active gust load alleviation systems for aircraft*. Ph.D. thesis, Politecnico di Milano.

[24] Yamashiro, H. and Stirling, R. (August 20–23 2007). Reduction of flight control system/structural mode interaction. AIAA Atmospheric Flight Mechanics Conference and Exhibit. Hilton Head, SC, USA. doi:10.2514/6.2007-6381. doi:10.2514/6.2007-6381.

[25] Kron, A., Lafontaine, J. d., and Alazard, D. (2003). Robust 2-dof H-infinity controller for highly flexible aircraft: Design methodology and numerical results. *Canadian Aeronautics and Space Journal*, 49(1), 19–29. doi:10.5589/q03-001. doi:10.5589/q03-001.

[26] Aouf, N., Boulet, B., and Botez, R. (2000). H_2 and H_∞ optimal gust load alleviation for a flexible aircraft. In *Proc. of American Control Conference*. Chicago, IL, USA.

[27] Fonte, F., Ricci, S., and Mantegazza, P. (2015). Gust load alleviation for a regional aircraft through a static output feedback. *Journal of Aircraft*, 52(5), 1559–1574. https://doi.org/10.2514/1.C032995.

[28] Sokolov, V. *Contributions to the minimal realization problem for descriptor systems*. Ph.D. thesis, Technical University Chemnitz, 2006.

[29] Lefteriu, S. and Antoulas, A. (2010). A new approach to modeling multiport systems from frequency-domain data. *IEEE Transactions on Computer-Aided Design of Integrated Circuits and Systems*, 29(1), 14–27. https://doi.org/10.1109/TCAD.2009.2034500.

[30] Quero, D., Vuillemin, P., and Poussot-Vassal, C. (2019). A generalized state-space aeroservoelastic model based on tangential interpolation. *Aerospace*, 6(1). ISSN 2226-4310. doi:10.3390/aerospace6010009. https://doi.org/10.3390/aerospace6010009.

[31] Köhler, M. (2014). On the closest stable descriptor system in the respective spaces RH_2 and RH_∞. *Linear Algebra and its Applications*, 443, 34–49. https://doi.org/10.1016/j.laa.2013.11.012.

[32] Theodorsen, T. (1935). General theory of aerodynamic instability and the mechanism of flutter. *NACA Technical Report 496*.

[33] Brunton, S. (2012). *Unsteady aerodynamic models for agile flight at low reynolds numbers*. Ph.D. thesis, Princeton University.

[34] Peters, D. (2008). Two-dimensional incompressible unsteady airfoil theory - an overview. *Journal of Fluids and Structures*, 24(3), 295–312. https://doi.org/10.1016/j.jfluidstructs.2007.09.001.

[35] Hodges, D. and Pierce, G. (2011). *Introduction to Structural Dynamics and Aeroelasticity*. Cambridge Aerospace Series. Cambridge University Press, 2nd ed. https://doi.org/10.1017/CBO9780511997112.

[36] Gerdin, M. (2006). *Identification and estimation for models described by differential-algebraic equations*. Ph.D. thesis, Institutionen för systemteknik.

[37] Jones, R. (1940). The unsteady lift of a wing of finite aspect ratio. NACA Technical Report 681.

[38] Eversman, W. and Tewari, A. (1991). Modified exponential series approximation for the Theodorsen function. *Journal of Aircraft*, 28(9), 553–557. https://doi.org/10.2514/3.46063.

[39] Filotas, L. (1969). Theory of airfoil response in a gusty atmosphere. Part I: Aerodynamic transfer function. Tech. rep., University of Toronto.

[40] Giesing, J., Rodden, W., and Stahl, B. (1970). Sears function and lifting surface theory for harmonic gust fields. *Journal of Aircraft*, 7(3), 252–255. https://doi.org/10.2514/3.44155.

[41] Garrick, I. E. (1938). On some reciprocal relations in the theory of nonstationary flows. NACA Technical Report 629.

[42] Quero, D. (2017). *An Aeroelastic Reduced Order Model for Dynamic Response Prediction to Gust Encounters*. Ph.D. thesis, Technical University of Berlin. http://dx.doi.org/10.14279/depositonce-6014.

[43] Kaiser, C., Freidewald, D., Quero, D., et al. (Braunschweig, Germany, September 13–15 2016). Aeroelastic gust load prediction based on time-linearized RANS solutions. Deutscher Luft- und Raumfahrtkongress.

[44] Poussot-Vassal, C., Quero, D., and Vuillemin, P. (Vienna, Austria, 2018). Data-driven approximation of a high fidelity gust-oriented flexible aircraft dynamical model. In *9th International Conference on Mathematical Modelling*. https://doi.org/10.1016/j.ifacol.2018.03.094.

[45] Beckert, A. and Wendland, H. (2001). Multivariate interpolation for fluid-structure-interaction problems using radial basis functions. *Aerospace Science and Technology*, 5(2), 125–134. https://doi.org/10.1016/S1270-9638(00)01087-7.

[46] Friedewald, D., Thormann, R., Kaiser, C., et al. (2018). Quasi-steady doublet-lattice correction for aerodynamic gust response prediction in attached and separated transonic flow. *CEAS Aeronautical Journal*, 9(1), 53–66. https://doi.org/10.1007/s13272-017-0273-0.

[47] Smith, T. A., Hakanson, J., Nair, S., et al. (2004). State-space model generation for flexible aircraft. *Journal of Aircraft*, 41(6), 1473–1481. https://doi.org/10.2514/1.14433.

[48] Reschke, C. (2006). *Integrated flight loads modelling and analysis for flexible transport aircraft*. Ph.D. thesis, University of Stuttgart.

[49] Klimmek, T. (2014). Parametric set-up of a structural model for FERMAT configuration aeroelastic and loads analysis. *Journal of Aeroelasticity and Structural Dynamics*, 3(2). https://doi.org/10.3293/asdj.2014.27.

[50] Vassberg, J., DeHaan, M., Rivers, M., et al. (2008). Development of a common research model for applied CFD validation studies. AIAA CFD Drag Prediction Workshop Updates. doi:10.2514/6.2008-6919. https://doi.org/10.2514/6.2008-6919.

[51] MSC (2004). *Aeroelastic Analysis User's Guide Version 68*. MSC.Software Corporation.

[52] Zhou, K., Doyle, J., and Glover, K. (1996). *Robust and optimal control*. Prentice hall New Jersey.

[53] Apkarian, P. and Noll, D. (2006). Nonsmooth H_∞ synthesis. *IEEE Transactions on Automatic Control*, 51(1), 71–86. ISSN 0018-9286. https://doi.org/10.1109/TAC.2005.860290.

[54] Poussot-Vassal, C., Vuillemin, P., and Quero, D. (Naples, Italy, 2019). A structured approach for input derivative index-2 descriptor dynamical model control. In *European Control Conference (accepted)*.

[55] Thormann, R. and Widhalm, M. (2013). Linear-frequency-domain predictions of dynamic-response data for viscous transonic flows. *AIAA Journal*, 51(11), 2540–2557. https://doi.org/10.2514/1.J051896.

[56] Antoulas, A., Ionita, A., and Lefteriu, S. (2012). On two-variable rational interpolation. *Linear Algebra and its Applications*, 436(8), 2889–2915. https://doi.org/10.1016/j.laa.2011.07.017.

[57] Gosea, I. and Antoulas, A. (2015). Model reduction of linear and nonlinear systems in the Loewner framework: A summary. In *Control Conference (ECC), 2015 European*. IEEE, pp. 345–349.

COPYRIGHT STATEMENT